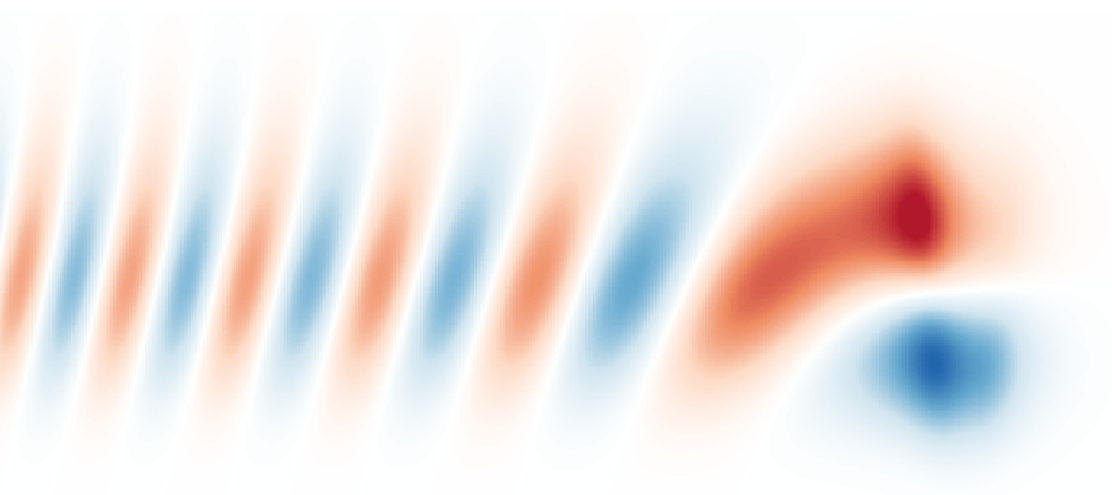


STRONG FIELD IONIZATION  
OF SMALL MOLECULES



JENS SVENSMARK  
PART A PROGRESS REPORT  
MAY 2014

SUPERVISOR: LARS BOJER MADSEN  
CO-SUPERVISOR: OLEG I. TOLSTIKHIN

DEPARTMENT OF PHYSICS AND ASTRONOMY  
AARHUS UNIVERSITY

# Preface

This progress report displays part of the work done during part A of my Ph.D. studies at the Department of Physics and Astronomy, Aarhus University.

The project so far falls into two parts. The first part, corresponding to the first year of my PhD study, is about solving the Time Dependent Schrödinger Equation (TDSE) using the split-step method. The second part, corresponding to the second year, is about the effects of nuclear motion on tunneling ionization in a static picture. The main focus of this progress report will be on the second part.

## Notation

Atomic units  $m_e = \hbar = e = 1$  are used throughout.

## Acknowledgements

I wish to thank my supervisor Lars Bojer Madsen for ideas, discussions and help getting a handle on the sometimes complicated issues of the project, and also for making all this possible.

I would also like to thank my co-supervisor Oleg I. Tolstikhin for giving important technical insight into the theory of tunneling ionization and his help shaping the project.

Finally I would like to thank Jens Egebjerg Bækthøj and Christian Kraglund Andersen for thorough proof reading of the manuscript.

# Contents

<b>Preface</b>	<b>i</b>
<b>Contents</b>	<b>ii</b>
<b>1 Introduction</b>	<b>1</b>
<b>2 Split-step</b>	<b>3</b>
2.1 Theory . . . . .	3
2.1.1 Propagation algorithm . . . . .	4
2.1.2 Imaginary time propagation . . . . .	5
2.1.3 Discretization and box . . . . .	5
2.1.4 3 dimensions . . . . .	6
2.1.5 Observables . . . . .	6
2.1.6 Plane wave projection . . . . .	6
2.2 Calculations . . . . .	6
2.2.1 Systems . . . . .	6
2.2.2 Results . . . . .	7
<b>3 Effects of nuclear motion on tunneling ionization</b>	<b>10</b>
3.1 Theory . . . . .	10
3.1.1 Exact solution . . . . .	12
3.1.2 Weak-field asymptotic theory . . . . .	15
3.1.3 Born-Oppenheimer approximation . . . . .	17
3.2 Model potentials . . . . .	18
3.2.1 Electronic potentials . . . . .	18
3.3 Results . . . . .	19
3.3.1 Wave function . . . . .	19
3.3.2 Finite range vs. coulomb potential . . . . .	21
3.3.3 Dipole . . . . .	24
<b>4 Outlook</b>	<b>27</b>
<b>Bibliography</b>	<b>29</b>

# 1 Introduction

Atoms and molecules and their interaction with light is one of the classic disciplines in physics, in which the focus traditionally has been on perturbation theory and time independent states [1]. Recent developments in laser technology has resulted in new ultrafast light sources, able to produce pulses with a duration of a few femto- or even hundreds of attoseconds [2]. These pulses are able to probe dynamics on the natural timescale of electron dynamics. The shortness of these pulses means that in addition to being very fast, these new light sources are also very intense, with field strengths comparable to the strength of the Coulomb interaction in atoms and molecules. These new experiments call for new non-perturbative theoretical methods and new time-domain methods.

When an atom or a molecule is exposed to a strong laser pulse, some of the electrons might escape and fly away. This process of electronic ionization is an important process in this new field known as attosecond physics; since the ionized electrons are observable, thus making comparison between experiment and theory possible. Furthermore, the challenge on the theory side with describing realistic atomic and molecular systems is a formidable one; even the simplest systems, such as He or H<sub>2</sub>, are not understood in complete detail.

For small systems fairly simple techniques, such as the split-step method [3], can be used to figure out how processes occur as time progresses. However, as the size of the systems under consideration increases, these simple methods become too computationally heavy for realistic use, and more complicated methods typically based on quantum chemistry methods such as e.g. the Multi-Configuration Time-Dependent Hartree-Fock (MCTDHF)[4] method must be used. Today the development of such methods is a very active field of research[5, 6, 7, 8].

If the electric field is not oscillating too quickly, the ionization process can be described in the quasi-static tunneling picture. More specifically, when the time it takes for an electron to tunnel from a molecule is short compared to the period of the laser field the dynamical process of ionization can be described in this tunneling picture. This picture is relevant for

describing processes in e.g. intense infrared laser fields [9].

In the limit of weak fields exact rates for tunneling ionization in a static uniform electric field can be obtained using the so called *Weak Field Asymptotic Theory* (WFAT) developed in [10, 11]. WFAT gives the tunneling ionization rate by an asymptotic expansion in the limit of weak fields. It has been applied to e.g. the tunneling ionization of linear molecules [12] and H<sub>2</sub>O [13] within the single active electron and frozen nuclei approximations. WFAT was recently generalized to also treat many-electron systems [14], but still in the frozen nuclei approximation.

When treating molecules the *Born-Oppenheimer* (BO) approximation is almost always used. It separates the electronic and nuclear degrees of freedom, and is the starting point for e.g. all methods used in quantum chemistry. In a recent paper Lars Bojer Madsen and Oleg I. Tolstikhin [15] showed that the BO approximation breaks down when describing static tunneling ionization in the weak field limit. This is explained as an effect of electron retardation. This paper also showed a way to generalize WFAT to the case of moving, non-frozen nuclei. This so called restructured WFAT gave the correct ionization rate in the weak field limit, and thus supplements the BO approximation, that fails in this limit.

The main focus of my project is to extend the results of [15]. In this paper a model potential with no coulomb tail was used, but since the potential of real molecules have a coulomb tail, an extension of the model to this case is desirable. [15] only treated a model homo-nuclear molecule with no dipole. Extending the model to hetero-nuclear molecules with a non-zero dipole is also desirable, as it allows for the description of more molecular systems.

Chapter 2 contains a description and shows some applications of the split-step method. It is rather simply implemented in Cartesian coordinates, but this also means that it is quite flexible and can easily treat for instance elliptically polarized light. This method has been around a while, and no new material is presented in this chapter. Chapter 3 is about nuclear effects on tunneling ionization. The material is an extension of previous theory, developed under the close supervision of Oleg I. Tolstikhin.

## 2 Split-step

In this chapter the theory of the split-step method will be introduced and some results of its application shown.

### 2.1 Theory

We wish to solve the Time Dependent Schrödinger Equation

$$i \frac{d}{dt} |\Psi(t)\rangle = H(t) |\Psi(t)\rangle. \quad (2.1)$$

Formally this can be solved using the time evolution operator  $U$ ,

$$|\Psi(t)\rangle = U(t, t_0) |\Psi(t_0)\rangle. \quad (2.2)$$

Using the time evolution operator we can propagate some initial state  $|\Psi(t_0)\rangle$  at time  $t_0$  to some final state  $|\Psi(t)\rangle$  at time  $t$ . The problem is that the form of the time evolution is not known in the general case, so we need to make some approximations.

For a time independent Hamiltonian  $H$  it is straightforward to show that the time evolution operator has the form of an exponential

$$U(t, t_0) = \exp[-iH \cdot (t - t_0)]. \quad (2.3)$$

The Hamiltonians we wish to consider are however not time independent, but if we assume that that Hamiltonian only varies a little over a time interval of size  $\Delta t$  we can to good approximation write the time evolution operator as a product of exponentials

$$U(t, t_0) \approx e^{-iH(t_0+(N-1)\Delta t)\cdot\Delta t} \dots e^{-iH(t_0+\Delta t)\cdot\Delta t} e^{-iH(t_0)\cdot\Delta t}, \quad (2.4)$$

where  $N\Delta t = t - t_0$ . The more subdivisions we make, the better is the above approximation. Propagation from time  $t_0$  to time  $t$  of the state  $|\Psi\rangle$  can be achieved applying the factors of the above expansion in succession to the initial state  $|\Psi(t_0)\rangle$ .

We assume the Hamiltonian can be separated into one part only dealing with momentum, and one dealing only with position

$$H(p, x) = T(p) + V(x). \quad (2.5)$$

The exponentials in (2.4) mix these parts, complicating the application of this operator. We can do a trick considering one of the factors of the approximation (2.4)

$$e^{-iH\Delta t} = e^{-i\frac{1}{2}V\Delta t} e^{-iT\Delta t} e^{-i\frac{1}{2}V\Delta t} + O(\Delta t^3). \quad (2.6)$$

This can be shown by expanding all exponentials according to  $e^x = \sum_{k=0}^{\infty} \frac{x^k}{k!}$  and comparing terms. In this way we can approximately express the time evolution operator as a product of factors that only depend on either position or momentum.

The final component that we need in order to do time-propagation is the Fourier transform. The wave function is the representation of the state in a position basis  $\Psi(x) = \langle x | \Psi \rangle$ . Similarly we have a corresponding momentum wave function  $\Psi(p) = \langle p | \Psi \rangle$ . One can change from one representation to the other using Fourier transforms

$$\Psi(p) = \frac{1}{\sqrt{2\pi}} \int_{-\infty}^{\infty} dx \Psi(x) e^{-ipx}, \quad (2.7)$$

$$\Psi(x) = \frac{1}{\sqrt{2\pi}} \int_{-\infty}^{\infty} dp \Psi(p) e^{ipx}. \quad (2.8)$$

### 2.1.1 Propagation algorithm

Propagation of the state  $|\Psi(t_0)\rangle$  to some later time  $|\Psi(t)\rangle$  can thus be done in the following way.

First we make  $N$  subdivisions, each of length  $\Delta t$ , of the time interval  $[t_0, t]$  such that  $N\Delta t = t - t_0$ . Starting with the state in position representation  $\Psi(x)$  the factor  $e^{-i\frac{1}{2}V\Delta t}$  of the time evolution operator is multiplied onto the wave function. This is easily done since the operator is diagonal in the position representation. Then the state is transformed to the momentum representation  $\Psi(p)$  using a Fourier transform. We can then apply the  $e^{-iT\Delta t}$  part of the time evolution operator to the  $\Psi(p)$  wave function, which again is easy, since the operator is diagonal in the momentum representation. We then Fourier transform back to the position representation  $\Psi(x)$  and apply the final factor of  $e^{-i\frac{1}{2}V\Delta t}$ . This procedure is then repeated  $N$  times with the final result being the wave function  $\Psi(x)$  at time  $t$ .

## 2.1.2 Imaginary time propagation

The method described in this chapter allows us to propagate a state  $|\Psi(t_0)\rangle$  from time  $t_0$  to some later time  $t$ . However, in order to propagate we need to know the initial state at time  $t_0$ . One choice of initial state to consider would be the stationary ground state of the system in a static picture. If the Hamiltonian is time-independent we can find stationary states as solutions to the time-independent Schrödinger equation

$$H|\Psi_n\rangle = E_n|\Psi_n\rangle. \quad (2.9)$$

The time evolution of the system is then given by

$$|\Psi(t)\rangle = \sum_n a_n e^{-iE_n t} |\Psi_n\rangle. \quad (2.10)$$

Let us consider this evaluated in negative imaginary time

$$|\Psi(-it)\rangle = \sum_n a_n e^{-E_n t} |\Psi_n\rangle. \quad (2.11)$$

As the time  $t$  goes by the term with the smallest energy gets bigger than the rest<sup>1</sup>. If enough time go by the smallest energy term will completely dominate the sum. Thus, by propagating in negative imaginary time we can obtain the stationary ground state, and the propagation can easily be done with the split-step method. To avoid the wave function attaining numerically unmanageable large values the wave function should be repeatedly renormalized during the imaginary time propagation.

## 2.1.3 Discretization and box

The wave functions described so far treats the position  $x$  and momentum  $p$  as continuous variables. However, we can not represent the wave function in infinitely many points in a computer. Instead we choose to discretize the  $x$  and  $p$  axes, using equidistant grids. These grids can not be extended indefinitely, so we terminate it at some point. This corresponds to choosing zero boundary conditions outside this 'box'. One effect of this discretization in a box is that integrals transforms into finite sums

$$\int_{-\infty}^{\infty} dx f(x) \rightarrow \sum_{i=1}^N \Delta x f(x_i). \quad (2.12)$$

The discretization of space is an approximation, but it gets better as the grid spacings  $\Delta x$  and  $\Delta p$  get smaller.

---

<sup>1</sup>For bound states  $E_n < 0$  and the exponential is growing



### 2.1.4 3 dimensions

In the preceding sections everything was expressed in terms of a 1 dimensional position coordinate  $x$ . The generalization of these results to three Cartesian coordinates  $x, y, z$  or  $x_1, x_2, x_3$  is straightforward and will not be covered.

### 2.1.5 Observables

Running a split-step propagation and seeing how the wave function evolves in time is interesting. But theoretical physics is about making predictions that can be tested by experiments, and the wave function can not be directly observed. So we need a way to extract some observable. In this work we will focus on electronic ionization, that is describing how the electrons leave the atom when exposed to an intense laser field. The typical quantity of interest in ionization is the momentum distribution of the ionized electrons. From this all other relevant observables, such as the spectrum, can be found.

### 2.1.6 Plane wave projection

The idea behind the plane wave projection method is that the ionizing electron becomes a collection of plane waves when it gets far away from the system from which it is ionizing. The momentum distribution can thus be obtained by doing a Fourier transform of the wave function after the pulse is done, and the outgoing wave packet has propagated some time. One limitation is that the wave packet must not reach the edge of the box, which due to computational limitations on the size of the box forces us to do the plane wave projection early, before the wave packet has reached the 'true' plane wave form. Also the parts of the wave function still bound after the ionization will never contribute to the ionization, so we need some way to remove these. The way we chose to do this was to put the wave function to zero within some radius around the origin after propagation. This will work assuming the bound states do not stretch too far out, and the unbound parts have had sufficient time to get away.

## 2.2 Calculations

### 2.2.1 Systems

So far everything has been put in quite general terms, without specifying the Hamiltonian. There is a reason for this. The code I have implemented

is quite flexible and can deal with a lot of different systems. Let us assume that we can write the Hamiltonian as

$$H(t) = H_0 + H_{\text{int}}(t), \quad (2.13)$$

where  $H_0$  is the Hamiltonian of the system with no external field and  $H_{\text{int}}(t)$  describes the interaction with the field. The field-free Hamiltonian  $H_0$  consists of two parts

$$H_0 = T + V \quad (2.14)$$

where the kinetic energy  $T = \frac{1}{2}\mathbf{p}^2$  and the potential  $V$  depends on the system. The code is rather flexible w.r.t. which potential we use. Any system with three coordinates can in principle be modelled. We can for instance model 1D Lithium or 3D Hydrogen. Another possibility is the 3D molecular hydrogen ion  $\text{H}_2^+$

$$V(\mathbf{x}) = -\frac{1}{\sqrt{(\mathbf{x} - \mathbf{R}/2)^2 + a^2}} - \frac{1}{\sqrt{(\mathbf{x} + \mathbf{R}/2)^2 + a^2}}, \quad (2.15)$$

where  $\mathbf{R}$  is a vector pointing from one nuclei to the other. We use a soft coulomb potential, since we can not handle the coulomb singularity in our discrete space representation.

The interaction with the field can be expressed in either length or velocity gauge. In velocity gauge the interaction Hamiltonian has form  $H_{\text{int}}(t) = \mathbf{A}(t) \cdot \mathbf{p}$ . Calculations have been done with an elliptically polarized pulse

$$\mathbf{A}(t) = A_0 \sin^2 \alpha t \begin{pmatrix} \cos\left(\omega t + \frac{\pi}{2}\left(1 - \frac{\omega}{\alpha}\right) + \varphi\right) \cos \frac{\epsilon}{2} \\ \sin\left(\omega t + \frac{\pi}{2}\left(1 - \frac{\omega}{\alpha}\right) + \varphi\right) \sin \frac{\epsilon}{2} \\ 0 \end{pmatrix}, \quad (2.16)$$

where  $\alpha = \frac{\omega}{2N}$  and  $N$  is the number of cycles in the pulse.

### 2.2.2 Results

See [http://users-phys.au.dk/jenssss/De1\\_A/](http://users-phys.au.dk/jenssss/De1_A/) for videos of the wave function.

Figure 2.1 shows the momentum distribution of the ionized electrons. The momentum distribution is a three dimensional quantity, thus the plot only shows a slice of this momentum distribution. A qualitative difference between the momentum distributions in the  $\beta = 0^\circ$  case, corresponding to the molecular axis being perpendicular to the polarization plane of the pulse, and the  $\beta = 90^\circ$  case is evident.

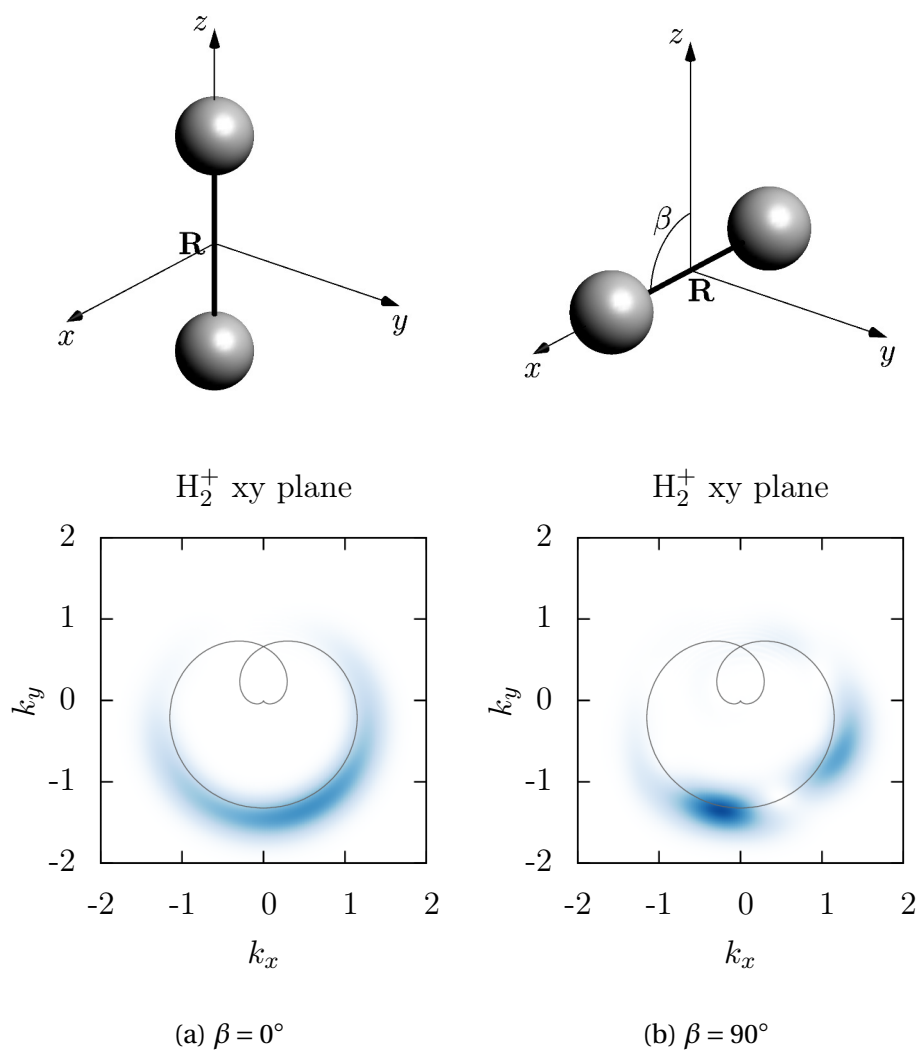


Figure 2.1: One plane of the momentum distribution of the ionized electrons for different orientations of the molecule. The field is circularly polarized in the  $xy$  plane. The gray trace shows the vector potential.

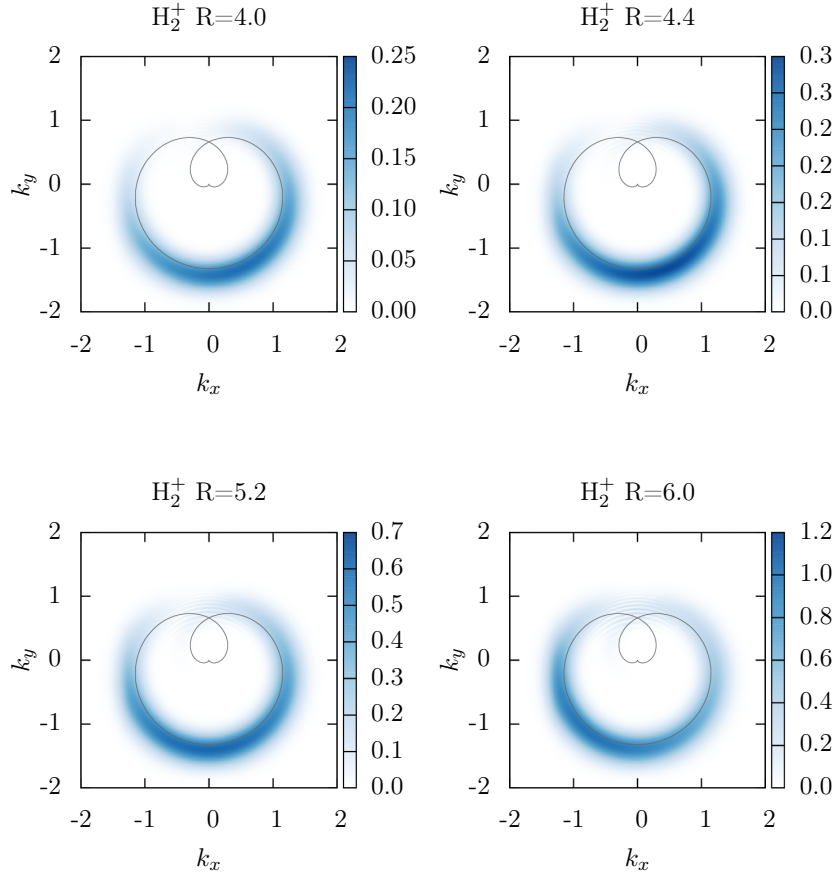


Figure 2.2: Momentum distribution of the ionized electrons for different inter-nuclear distances  $R$ . The field is circularly polarized in the  $xy$  plane.  $A_0 = 1.872$ ,  $\omega = 0.056$ ,  $\beta = 0^\circ$ . The gray trace shows the vector potential.

Figure 2.2 shows the momentum distribution for different values of the inter-nuclear distance  $R$ . It is seen that as the inter-nuclear distance is increased from  $R = 4.0$  to  $R = 6.0$ , the peak of the momentum distribution shifts from pointing left to pointing right.

One problem with this method is the scaling of calculations. If we for instance use 1024 points in each of the 3 dimensions, storing the wave function in double precision would take up about 16 gigabytes of memory and a time propagation calculation take about a week. This resolution is however not sufficient for describing electronic ionization in a near-infrared laser field, which is the regime in which we have theoretical explanations for the effects observed in figures 2.1 and 2.2. Pushing the resolution any higher is computationally unfeasible.

# 3 Effects of nuclear motion on tunneling ionization

In chapter 2 we considered solutions of the time-dependent Schrödinger equation as 'wave packets'. Here we consider the time-independent Schrödinger equation and its stationary solutions. The work presented in this chapter is a continuation of the work presented in ref. [15] by Lars Bojer Madsen and Oleg I. Tolstikhin. My contributions have been to extend ref. [15] to systems with a coulomb tail and a dipole.

The process we describe is tunneling ionization. The main observable for describing this is the ionization rate  $\Gamma$ , expressing how quickly the electron leaves the molecule. In ref. [15] two different approximations were used for finding the rate, the BO approximation accurate at large field strengths and WFAT accurate at weak fields. We consider a simple 1D model system, designed to emulate  $H_2$ , for which we can find the rate exactly. This exact rate can then be compared with the rates obtained in the WFAT and BO approximations, such that the performance of these approximations can be evaluated.

## 3.1 Theory

Consider a 1D model of a three-body system. The masses of the three particles are denoted  $m_1, m_2$  and  $m_3$ . Particles 1 and 2 are heavy nuclei, while particle 3 is an electron. Atomic units are used, so  $m_3 = 1$ . The nuclei have charges  $q_1, q_2$ , the electron a charge  $q_3 = -1$ . We consider the particles in a center-of-mass system with coordinates  $x_1, x_2$  and  $x_3$  that fulfill  $m_1 x_1 + m_2 x_2 + m_3 x_3 = 0$ . Let us introduce the reduced masses

$$m = \frac{m_1 + m_2}{m_1 + m_2 + m_3}, \quad M = \frac{m_1 m_2}{m_1 + m_2}, \quad (3.1)$$

effective charges

$$q = \left( \frac{q_1 + q_2}{m_1 + m_2} - \frac{q_3}{m_3} \right) m_3 m, \quad Q = -M \left( \frac{q_2}{m_2} - \frac{q_1}{m_1} \right), \quad (3.2)$$

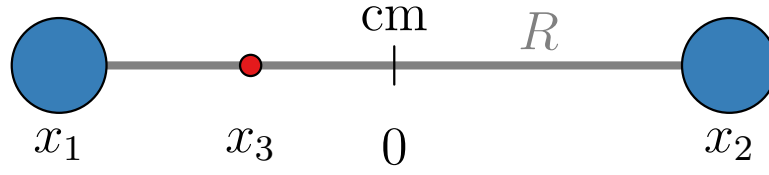


Figure 3.1: Three-body center-of-mass system with the two heavy nuclei (blue) at  $x_1$  and  $x_2$  and the light electron (red) at  $x_3$ .  $R = x_2 - x_1$  is the internuclear coordinate.

and the Jacobi coordinates

$$R = x_2 - x_1, \quad x = x_3 / m. \quad (3.3)$$

Expressed in terms of these the systems Schrödinger equation reads

$$\left[ -\frac{1}{2M} \frac{d^2}{dR^2} - \frac{1}{2m} \frac{d^2}{dx^2} + U(R) + V(x, R) + F(QR + qx) - E(F) \right] \Psi(x, R) = 0. \quad (3.4)$$

The model internuclear  $U(R)$  and electronic  $V(x, R)$  potentials emulate a single active electron (SAE) model and their exact form will be specified in section 3.2. For now we consider a  $U(R)$  that has no continuum, that is, it only supports a discrete spectrum. This has important effects on the dynamics of the system, but we postpone a study of the disassociation channel since the problem is still very interesting without this channel and remains basically unexplored. Additionally we assume that the nuclei can not pass through each other, so the variables in equation (3.4) vary in the intervals  $-\infty < x < \infty$  and  $0 \leq R < \infty$ .

The potential  $U(R)$  should model a positive molecular ion with the total charge  $q_1 + q_2 = 1$ . This choice makes the present center-of-mass frame inertial.

We solve (3.4) subject to zero boundary conditions in  $R$

$$\Psi(x, 0) = \Psi(x, R \rightarrow \infty) = 0, \quad (3.5)$$

and for  $F \geq 0$  zero boundary condition in the  $x \rightarrow \infty$  limit

$$\Psi(x \rightarrow \infty, R) = 0. \quad (3.6)$$

At  $x \rightarrow -\infty$  we impose outgoing-wave boundary conditions to be specified later. With these boundary conditions we have defined an eigenvalue problem. The solutions to this eigenvalue problem are called Siegert States (SS) [10]. The eigenvalue is complex

$$E(F) = \mathcal{E}(F) - \frac{i}{2}\Gamma(F), \quad (3.7)$$

and the eigenfunction is normalized by

$$\int_0^\infty dR \int_{-\infty}^\infty dx \Psi^2(x, R) = 1. \quad (3.8)$$

### 3.1.1 Exact solution

#### Reduction to a multi-channel eigenvalue problem

In order to solve eq. (3.4) we introduce a complete set of vibrational states of the molecular ion, the so called *adiabatic basis*

$$\left[ -\frac{1}{2M} \frac{d^2}{dR^2} + U(R) + FQR - \varepsilon_\nu(F) \right] \varphi_\nu(R) = 0, \quad \nu = 0, 1, 2, \dots, \quad (3.9)$$

with boundary conditions  $\varphi_\nu(0) = 0$ , expressing that we do not allow the nuclei to pass through each other, and  $\varphi_\nu(\infty) = 0$  expressing that we do not allow disassociation of the molecule.

The adiabatic basis functions  $\varphi_\nu(R)$  and their eigenvalues  $\varepsilon_\nu(F)$  are real and the basis functions are orthonormal

$$\int_0^\infty dR \varphi_\nu(R) \varphi_{\nu'}(R) = \delta_{\nu\nu'}. \quad (3.10)$$

The wave function  $\Psi(x, R)$  is expressed in the adiabatic basis as

$$\Psi(x, R) = \sum_\nu f_\nu(x) \varphi_\nu(R). \quad (3.11)$$

Inserting the wave function (3.11) in the Schrödinger equation (3.4), and projecting on the  $\varphi_\nu(R)$  basis yields

$$\left[ -\frac{1}{2m} \frac{d^2}{dx^2} + Fqx + \varepsilon_\nu(F) - E(F) \right] f_\nu(x) + \sum_{\nu'} V_{\nu\nu'}(x) f_{\nu'}(x) = 0, \quad (3.12)$$

where  $V_{\nu\nu'}(x) = \int_0^\infty dR \varphi_\nu(R) V(x, R) \varphi_{\nu'}(R)$ . By projecting out the  $R$  degree of freedom we thus obtain a system of coupled equations for the *coefficient functions*  $f_\nu(x)$ . Let us consider our problem in the limit  $|x| \rightarrow \infty$ . We assume that our potential in this limit has mono-pole form

$$V(x, R) = -\frac{Z}{|x|} + O(x^{-2}) \quad (3.13)$$

In this asymptotic limit the potential is independent of  $R$ , thus the channel equations (3.12) decouple

$$\left[ -\frac{1}{2m} \frac{d^2}{dx^2} + Fqx - \frac{Z}{|x|} + \varepsilon_\nu(F) - E(F) \right] f_\nu(x) = 0. \quad (3.14)$$

The asymptotic solution to this equation can be constructed. In the case where  $F = 0$  the leading order term of this asymptotic have the form

$$f_\nu(x)|_{x \rightarrow -\infty} = g_\nu(-x)^{\alpha_\nu} e^{-\varkappa_\nu(-x)}, \quad \varkappa_\nu = \sqrt{2m[\varepsilon_\nu(0) - E(0)]}, \quad (3.15)$$

where  $\alpha_\nu = mZ/\varkappa_\nu$  and the asymptotic coefficient  $g_\nu$  is a constant specific for each channel.

For  $F > 0$  the leading term of the solutions satisfying outgoing-wave boundary conditions have the asymptotic form in the  $x \rightarrow -\infty$  limit

$$f_\nu(x)|_{x \rightarrow -\infty} = f_\nu \frac{m^{1/4}}{(2Fq(-x))^{1/4}} \times \exp \left[ i \frac{(2m)^{1/2}}{(Fq)^{1/2}} \left( \frac{2}{3} Fq(-x)^{3/2} + (E(F) - \varepsilon_\nu(F))(-x)^{1/2} \right) \right]. \quad (3.16)$$

In the  $x \rightarrow \infty$  limit, the  $f_\nu(x)$  coefficient functions vanish.

When no field is present, the Schrödinger equation (3.4) with boundary conditions (3.15) can be solved. Expressing the Hamiltonian in a product basis of the spectral basis  $\varphi_\nu$  and a spatial Discrete Variable Representation (DVR) [16] basis within some sufficiently large box in  $x$ , this Hamiltonian can be directly diagonalized. When we do a direct diagonalization in a box we implicitly assume that the wave function goes to zero at the box boundary. This is indeed a very good approximation for bound states when no field is applied. However, when a static field is present, the wave function does not go to zero at both box edges. At one edge the potential grows indefinitely deep and the wave function will be non-zero for arbitrarily large  $|x|$ , as illustrated in figure 3.2. A different approach is needed when a field is applied.

### R-matrix propagation

In this work we use the R-matrix propagation method [17]. The R-matrix is essentially the ratio of the wave function and its derivative. The R-matrix  $\mathcal{R}$  is defined such that

$$f_\nu(x) = \sum_{\nu'} \mathcal{R}_{\nu\nu'}(x; E) \frac{d}{dx} f_{\nu'}(x). \quad (3.17)$$

The R-matrix propagation method consists of dividing the  $x$  axis into a series of sectors. A spatial Legendre DVR [18] basis is chosen in each sector, and the local Hamiltonian is diagonalized by means of the *slow variable discretization* (SVD) method [19]. Based on this diagonalization the R-matrix can be propagated from sector to sector. Details of this is described in the appendix of [20].



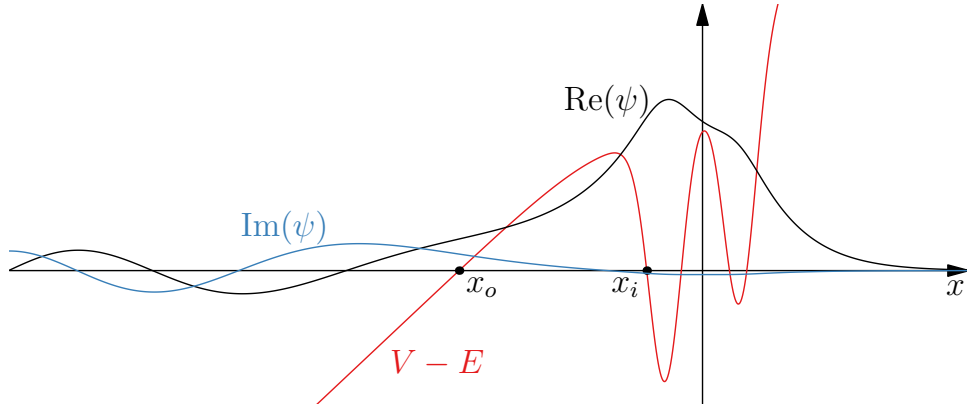


Figure 3.2: SS eigenfunction at  $R = 1.4$  a.u. with field, illustrating the concepts of inner ( $x_i$ ) and outer ( $x_o$ ) turning points, outgoing wave and classically forbidden region.

Before we can propagate the R-matrix we need some initial R-matrix. This is obtained asymptotically. Since the channel equations (3.12) decouple in the large  $|x|$  limit the R-matrix is diagonal and has the form

$$\mathcal{R}_{vv'}(x; E)|_{|x| \rightarrow \infty} = \frac{f_v(x)}{\frac{d}{dx} f_v(x)} \delta_{vv'}. \quad (3.18)$$

The coefficient function  $f_v(x)$  and its derivative can be found in this asymptotic region using the asymptotic expansion mentioned after equation (3.14).

The method we employ is the following; first we pick some initial energy based on a direct diagonalization of the field-free Hamiltonian. Then we take a small step in field strength and find the asymptotic R-matrices at the right and left ends of our box. These are then propagated through the sectors until they meet at some matching point  $x_0$  near the center of the box. Since the potentials considered are smooth, the coefficient functions must be continuous and their derivatives like so. This implies that the matrix difference of the R-matrices propagated from the left and from the right must have a zero eigenvalue, such that this difference matrix is singular

$$\det [\mathcal{R}_{\text{left}}(x_0; E) - \mathcal{R}_{\text{right}}(x_0; E)] = 0. \quad (3.19)$$

We then find the zero of this determinant by doing a simple Newton search with the energy  $E$  as variable. In each step a new guess for the energy is obtained, which is then used to construct the asymptotic R-matrices etc. This proceeds until the energy giving the zero eigenvalue is found. Then a

new step in  $F$  is made and the procedure is repeated, this time using the present energy as a guess for the new energy.

The eigenvector belonging to the zero eigenvalue of the R-matrix difference matrix is the derivative of the wave function, from which we can construct the entire wave function.

### 3.1.2 Weak-field asymptotic theory

Weak field asymptotic theory (WFAT) gives the ionization rate in the limit of very weak fields. The theory gives a connection between the asymptotic coefficients of the wave function in the field-free and weak-field cases. These asymptotic coefficients are linked to the ionization rate, and thus WFAT yields the ionization rate in the weak-field limit based entirely on field-free quantities.

#### Asymptotic coefficients and ionization rate

The ionization rate  $\Gamma$  is the main observable we are concerned with. Consider the time-dependent Schrödinger equation (TDSE)

$$i \frac{d}{dt} \Psi = H \Psi. \quad (3.20)$$

with a Hamiltonian of the form

$$H = -\frac{1}{2m} \frac{d^2}{dx^2} - \frac{1}{2M} \frac{d^2}{dR^2} + V(x, R) \quad (3.21)$$

Using the TDSE together with its conjugate equation we obtain

$$\frac{d}{dt} |\Psi|^2 = \frac{d}{dx} j_x + \frac{d}{dR} j_R, \quad (3.22)$$

where the currents are defined as

$$j_x = \frac{1}{i2m} \left( \Psi \frac{d}{dx} \Psi^* - \Psi^* \frac{d}{dx} \Psi \right), \quad (3.23)$$

$$j_R = \frac{1}{i2M} \left( \Psi \frac{d}{dR} \Psi^* - \Psi^* \frac{d}{dR} \Psi \right). \quad (3.24)$$

The ionization rate is a measure of how quickly probability flows out of a region surrounding the molecule<sup>1</sup>

$$\Gamma = \frac{1}{N(b, a)} \frac{d}{dt} \int_a^b dx \int_0^\infty dR |\Psi(t)|^2 \quad (3.25)$$

$$= \frac{1}{N(b, a)} \sum_v (j_v(b) - j_v(a)), \quad (3.26)$$

<sup>1</sup>We do not consider disassociation of the nuclei, so the integration over  $R$  simply runs over the whole range of  $R$ .

where  $N(b, a) = \int_a^b dx \int_0^\infty dR |\Psi(t)|^2$  is the amount of probability between  $x = a$  and  $x = b$ , and the channel current is defined as

$$j_\nu = \frac{1}{i2m} \left( f_\nu \frac{d}{dx} f_\nu^* - f_\nu^* \frac{d}{dx} f_\nu \right). \quad (3.27)$$

We consider the current in the asymptotic region  $x \rightarrow -\infty$  and insert the asymptotic form from equation (3.16). Furthermore we assume  $\text{Im}(E) = 0$ , which is approximately true in the weak field limit, and we obtain

$$j_\nu(x \rightarrow -\infty)|_{F \rightarrow 0} = |f_\nu|^2. \quad (3.28)$$

We define partial rates as the norm square of the asymptotic coefficients

$$\Gamma_\nu \equiv |f_\nu|^2. \quad (3.29)$$

The total rate in the weak-field limit is then

$$\Gamma|_{F \rightarrow 0} = \sum_\nu \Gamma_\nu \quad (3.30)$$

If we have a stationary state  $\Psi_0$  the time evolution is given by  $\Psi(t) = e^{-iEt} \Psi_0$ , and in this case the rate is

$$\Gamma = -2 \text{Im} E. \quad (3.31)$$

In WFAT we consider the limit of weak fields. We therefore expand all quantities to first order in the field. The total energy is

$$E(F) = E(0) - \mu F + O(F^2), \quad (3.32)$$

where the dipole moment  $\mu$  can be calculated from the field free wave function

$$\mu = - \int_0^\infty dR \int_{-\infty}^\infty dx (QR + qx) \Psi^2(x, R). \quad (3.33)$$

The diabatic channel energies  $\varepsilon_\nu(F)$  also depends on the field and should likewise be expanded

$$\varepsilon_\nu(F) = \varepsilon_\nu(0) - \mu_\nu^R F + O(F^2), \quad (3.34)$$

where

$$\mu_\nu^R = - \int_0^\infty dR QR \varphi_\nu^2(R). \quad (3.35)$$

A derivation<sup>2</sup> similar to that in [10] yields a partial rate

$$\Gamma_\nu = |f_\nu|^2 = G_\nu^2 W_\nu(F) [1 + O(F)], \quad (3.36)$$

where the field factor  $W_\nu(F)$  and structure factor  $G_\nu$  are defined as

$$W_\nu(F) = \frac{\varkappa_\nu}{m} \left( \frac{2\varkappa_\nu^2}{mFq} \right)^{\frac{2mZ}{\varkappa_\nu}} \exp\left(-\frac{2\varkappa_\nu^3}{3mFq}\right), \quad (3.37)$$

$$G_\nu = g_\nu \exp\left(-\frac{\varkappa_\nu}{q} \mu_\nu\right), \quad (3.38)$$

where  $\mu_\nu = \mu - \mu_\nu^R$ .

WFAT is applicable when the field is weaker than

$$F \ll F_c \approx \frac{\varkappa_\nu^4}{4m^2 Z q}. \quad (3.39)$$

### 3.1.3 Born-Oppenheimer approximation

In the Born-Oppenheimer (BO) approximation the nuclear masses are assumed to be very much larger than the electronic mass. In this limit  $m = 1$ . The wave function becomes a simple product  $\Psi(x, R) = \chi(R)\psi_e(x; R)$ , where the electronic wave function  $\psi_e(x; R)$  depends on  $R$  parametrically. The two factors of the wave function fulfills the equations

$$\left[ -\frac{1}{2} \frac{d^2}{dx^2} + V(x, R) + Fqx - E_e(R; F) \right] \psi_e(x; R) = 0, \quad (3.40)$$

$$\left[ -\frac{1}{2M} \frac{d^2}{dR^2} + U(R) + FQR + E_e(R; F) - E_{\text{BO}}(F) \right] \chi(R) = 0. \quad (3.41)$$

For  $F > 0$  the electronic equation (3.40) is subject to outgoing-wave boundary conditions in the  $x \rightarrow -\infty$  limit

$$\begin{aligned} \psi_e(x; R)|_{x \rightarrow -\infty} &= f_{\text{BO}}(R) \frac{1}{(2Fq(-x))^{1/4}} \\ &\times \exp\left[ i \frac{2^{1/2}}{(Fq)^{1/2}} \left( \frac{2}{3} Fq(-x)^{3/2} + E_e(R; F)(-x)^{1/2} \right) \right] \end{aligned} \quad (3.42)$$

and vanishing  $\psi_e(x; R)$  in the  $x \rightarrow \infty$  limit. The nuclear equation (3.41) is subject to the boundary conditions  $\chi(0) = \chi(\infty) = 0$ .

The electronic equation (3.40) is solved using the same R-matrix propagation technique as described in section 3.1.1. The nuclear equation (3.41) is then solved by direct diagonalization in a DVR basis.

<sup>2</sup>This derivation is to be included in an appendix of an upcoming paper

## 3.2 Model potentials

The inter-nuclear interaction is modeled by the potential

$$U(R) = \frac{A}{R^2} + B + CR^2, \quad (3.43)$$

with coefficients  $A = 0.26$ ,  $B = -0.732635$  and  $C = 0.01625$ . These are chosen to reproduce the BO potential of  $H_2^+$  as shown by the red lines in figure 3.3. This internuclear potential does not have continuum states, that is we do not consider disassociation of the molecule.

### 3.2.1 Electronic potentials

The interaction between the nuclei and the electron is modeled by a potential of the form

$$V(x, R) = V_1 \left( x + \frac{m_2}{m_1 + m_2} R \right) + V_2 \left( x - \frac{m_1}{m_1 + m_2} R \right). \quad (3.44)$$

In ref. [15] a finite range potential

$$V_i(x) = -\frac{a}{\cosh^2(bx)} \quad (3.45)$$

with parameters  $a = 0.62772$  and  $b = 0.857$  was used. This potential will be referred to as frp (Finite Range Potential).

In this work we additionally consider a potential with a coulomb tail, referred to as ctp (Coulomb Tail Potential). It has the form

$$V_i(x) = -q_i \frac{1 - d e^{-fx^2}}{\sqrt{x^2 + a^2}} - c e^{-bx^2} \quad (3.46)$$

with parameters  $a = 1$ ,  $b = 5.46$ ,  $c = 0.931$ ,  $d = 0.633$ ,  $f = 0.0402$  and  $q_1 = q_2 = 0.5$ . These parameters are chosen such that the BO potential reproduces the BO potential of  $H_2$  (black curves in figure 3.3). Asymptotically the electronic potential reduces to the form

$$V(x, R)|_{x \rightarrow \pm\infty} = -\frac{q_1 + q_2}{|x|}. \quad (3.47)$$

Since this situation corresponds to an electron effectively having left the  $H_2^+$  molecular ion we naturally require that  $q_1 + q_2 = 1$ .

We also consider a third electronic potential, the capped ctp (cctp). For this we define a function which is 1 close to the center and goes continuously to zero outside some region

$$f(x) = \begin{cases} \exp(-(|x| - 10)^2/10) & |x| > 10 \\ 1 & \text{else.} \end{cases} \quad (3.48)$$

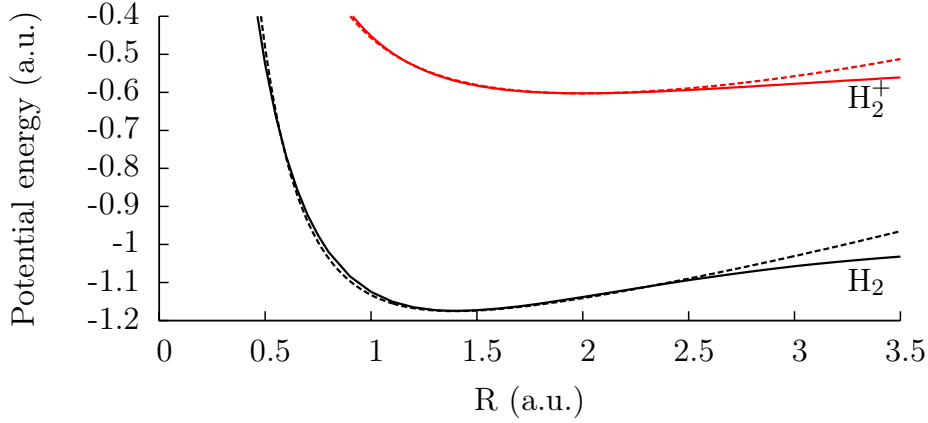


Figure 3.3: Solid lines: BO potentials for  $H_2^+$  [21] and  $H_2$  [22] as functions of the internuclear distance  $R$ . Dashed lines: present model internuclear potential  $U(R)$  (upper) and BO potential for the three-body system  $U(R) + E_e(R, 0)$  (lower).

We still use the ctp potential but modify the electronic potential equation (3.44) by multiplying this function

$$V(x, R) = f(x) \cdot \left[ V_1 \left( x + \frac{m_2}{m_1 + m_2} R \right) + V_2 \left( x - \frac{m_1}{m_1 + m_2} R \right) \right]. \quad (3.49)$$

The purpose of this is to get a potential that is the same as the ctp potential near the nuclei, where most of the wave function is located, but does not have a coulomb tail.

Figure 3.4 shows the frp and ctp potentials at the  $H_2$  equilibrium distance  $R_0 = 1.4$  a.u. and illustrates that the frp and ctp potentials are qualitatively different, as frp has one minimum at  $R_0$ , whereas ctp has two. The figure also shows that at  $x = 10$  a.u. where the potential is capped in cctp, the wave function has decayed to a very small value.

## 3.3 Results

### 3.3.1 Wave function

It is possible to extract the wave function from the R-matrix propagation. Figure 3.5 shows the real and imaginary parts of the wave function when a field is present. The outgoing wave pattern is evident in this figure and the wave fringes are slanted. The slanting of these fringes is a phenomena we might look closer at later.

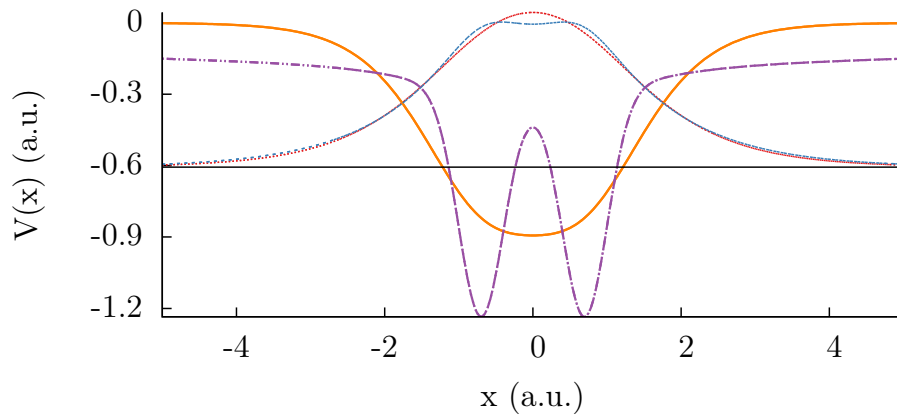


Figure 3.4: Solid orange (dashed-dotted purple) line: potential for the frp (ctp) potential at  $R_0 = 1.4$  a.u.. Dotted red (dashed blue) line: ground state electronic wave function at this  $R_0$  for the frp (ctp) potential, the solid black line is the energy of these ground states (the energies are almost the same).

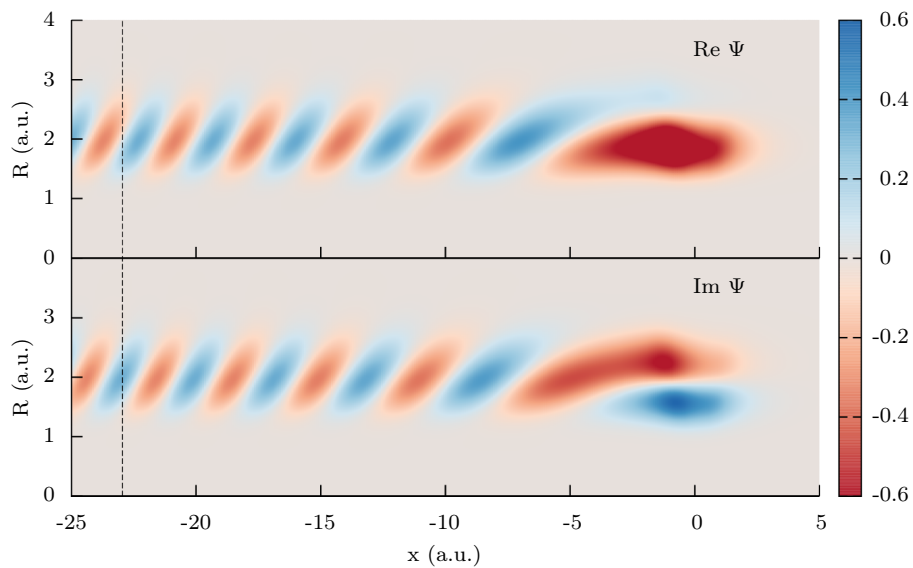


Figure 3.5: Real and imaginary parts of the SS eigenfunction for the ctp potential at  $F = 0.134$  a.u.. The dashed line is a guide for the eye, to facilitate comparison of the two parts of the wave function. It is seen that the imaginary part is about one quarter of period ahead of the real part in the negative  $x$  direction, as it should be for an outgoing wave.

### 3.3.2 Finite range vs. coulomb potential

The ionization rate has been determined for the different model potentials at different field strengths. The results are shown in figure 3.6. The exact rates are as  $\Gamma = -2\text{Im}(E)$ , where  $E$  is the energy obtained from R-matrix propagation.

The BO rate was likewise found from  $\Gamma_{\text{BO}} = -2\text{Im}(E_{\text{BO}})$ , where the BO energy,  $E_{\text{BO}}$ , was obtained by solving the BO problem in eqs. (3.40) and (3.41). From ref. [15] we expect that BO will work well for large  $F$ , but fail at small  $F$ , which is indeed what is seen in figure 3.6.

The WFAT rate is obtained by summing the partial WFAT rates from eq. (3.36). The WFAT approximation is exact in the  $F \rightarrow 0$  limit.

Figure 3.6a shows rates for the frp potential. This potential was also used in ref. [15], and indeed this figure is the same as figure 3 of this article. One remarkable feature of these rates is that the exact and WFAT results agree over a very large range of  $F$  as they stay together up to around  $F = 0.1$  a.u. Figure 3.6c shows the same for the ctp potential. Here the exact and WFAT rates start to differ at somewhat smaller  $F$ , around 0.02 a.u. One of the main differences between the frp and ctp potentials is that ctp has a coulomb tail, whereas frp does not. One might be tempted to conclude that the difference between these potentials is due to the coulomb tail, but it seems that other factors play a larger role, as will be explained.

In [11] the form of WFAT derived in this work is labeled as zeroth order WFAT, since it only considers the wave function to zeroth order in field. This reference develops first order WFAT, where first order field corrections to the wave function are considered. A number of effects contribute to the first order WFAT correction, one of them is the wave function field distortion. Figure 3.7 shows the norm square of the wave function for the two potentials with and without field. It is evident that the ctp wave function is distorted a lot more by the field than the frp wave function, and we would therefore expect that at least this contribution to the first order WFAT correction is larger for ctp than frp.

To thoroughly demonstrate that the difference in how well the WFAT approximation gives the exact rates in the frp and ctp cases is not related to the coulomb tail we consider the cctp potential. Figure 3.6e shows that the WFAT ionization rate departs from the exact rate for  $F$  comparable to that for ctp. The cctp potential is without a coulomb tail, but with the same form as ctp near the nuclei, so figure 3.6e demonstrates that the agreement between WFAT and exact results in the frp case is not due to the lack of coulomb tail.

More details about the origin of the first order WFAT corrections is beyond the scope of this work, but we can make a comment on the size



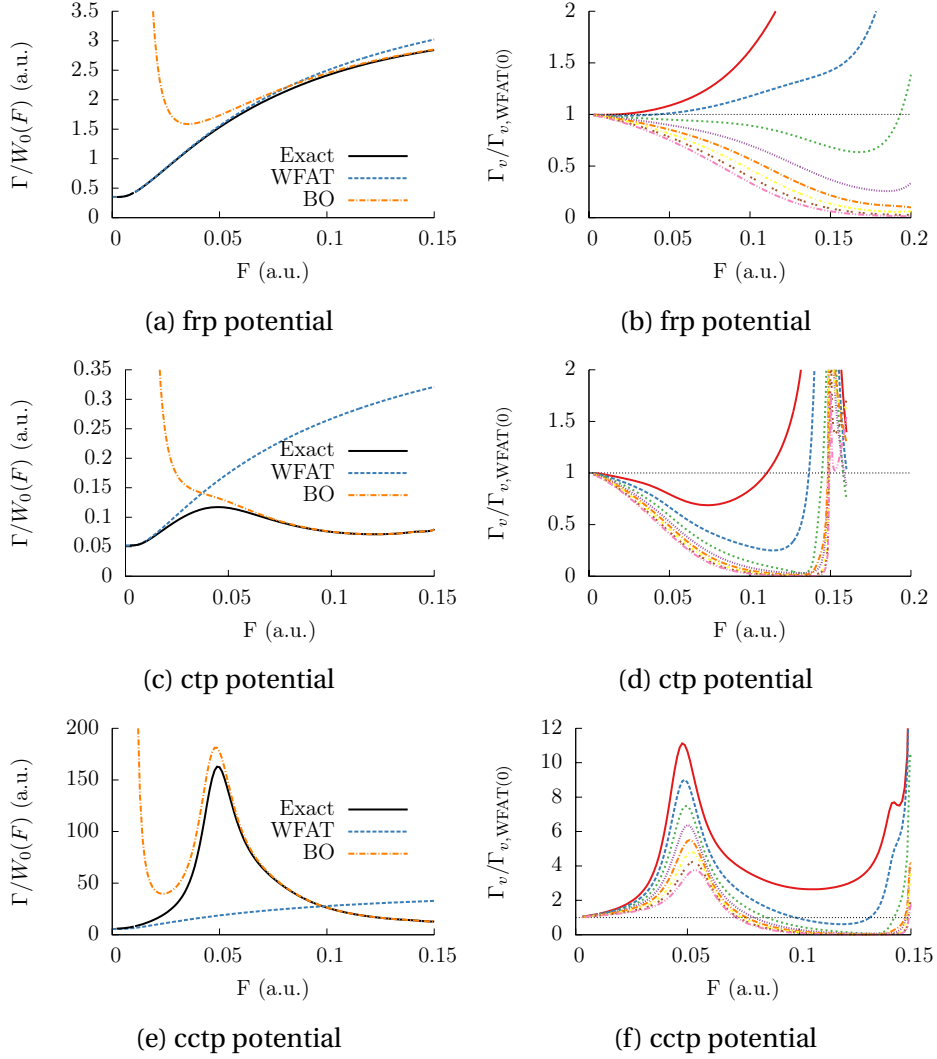


Figure 3.6: (a),(c),(e): Ionization rate of the ground state divided by the field factor for the zeroth channel  $W_0(F)$ , eq. (3.37).

(b),(d),(f): Exact partial rates  $\Gamma_\nu = |f_\nu|^2$  divided by the WFAT partial rates  $\Gamma_{\nu,\text{WFAT}} = G_\nu^2 W_\nu(F)$ , see equation (3.36). The red line is the first channel, the rest follow in order downwards. The dotted line at 1 is a guide for the eye.

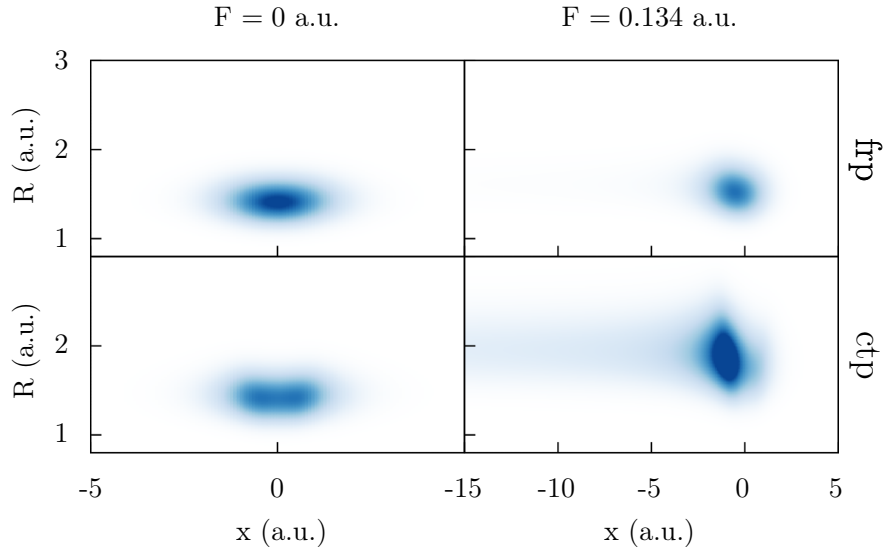


Figure 3.7: Norm square of wave function displaying the amount of wave function field distortion for the frp and ctp potentials. It is seen that the ctp potential is distorted a lot more than the frp potential.

of these corrections. The asymptotic coefficients  $f_\nu$  in terms of which the partial rates  $\Gamma_\nu = |f_\nu|^2$  are defined can be obtained exactly from the R-matrix propagation, since we can construct the wave function. These exact partial rates are compared to their WFAT counterparts in figure 3.6. The plots in this figure show  $\Gamma_\nu / (G_\nu^2 W_\nu(F))$ , so from equation (3.36) we see that this corresponds to  $1 + O(F)$ . This curve essentially shows the error of WFAT for each channel by how much each curve departs from 1. In the  $F \rightarrow 0$  limit all these curves should approach 1, which they indeed appear to be doing. Interestingly we see that the partial rates for the frp potential have a slope, that is a first order WFAT correction, close to zero for all channels, while the ctp potential have a more substantial slope.

As a technical note it should be mentioned, that floating point number precision is an issue when the rate for small field strengths is to be determined. From equation (3.36) we see that the rate becomes exponentially small as  $F \rightarrow 0$ . At  $F \approx 0.02$  a.u. the imaginary part of the energy is about  $\text{Im}(E) \approx 10^{-15}$ . The real part of the energy is about order 1, so the imaginary part relative to the real part of the energy is  $10^{-15}$ , which is comparable to the relative accuracy of the standard double precision (64 bit) numbers. Thus using double precision numbers we can only get accurate rates for  $F > 0.02$  a.u.. A version of the code using the less standard quadruple (quad, 128 bit) precision numbers has been implemented.

With these quad precision numbers accurate exact rates can be obtained for smaller field strengths. There is, however, still a lower limit to how far down in field strength we can go.

### 3.3.3 Dipole

Asymmetry in  $x$  can be introduced into the model by choosing  $q_1 \neq q_2$ . Because of the asymptotic form of the potential in equation (3.47) we require that  $q_1 + q_2 = 1$ . The case  $q_1 = q_2 = 0.5$  corresponds to no asymmetry in  $x$  and the dipole is  $\mu = 0$  in this case.

Figure 3.8 shows the rate obtained from calculations using different values of  $q_1$ , with  $q_2 = 1 - q_1$ . For  $q_1 = 1$  the curve continues all the way to the edge of the plot, whereas for all the other  $q$ 's the curves terminate at smaller  $F$ . The termination of these curves demonstrates one of the issues of the R-matrix propagation method. Figure 3.9 shows the real part of the energies for a number of excited states. We see that the curves in figure 3.8 terminate corresponding to places where the real part of the energy cross with that of another state. At such places it is difficult for the R-matrix propagation algorithm to know which branch to follow, which causes its termination.

In all cases we get the expected behavior from BO; agreement at large  $F$  but difference at small  $F$ .

As the dipole increases we see that WFAT becomes increasingly bad. This is not completely unexpected. In the WFAT derivation, see [10], terms in the potential of order  $O(x^{-2})$  or greater was neglected. In the non-dipole case no  $O(x^{-2})$  terms exists in the potential so what we neglect is of order  $O(x^{-3})$  or greater. In the dipole cases a term of order  $O(x^{-2})$  is present in the potential, and the neglected terms are therefore of greater importance here.

Figure 3.9 shows the partial rates for the different dipole cases. We see that the first order WFAT correction, that is the slope of these curves near  $F = 0$ , is indeed smallest for the non-dipole  $q_1 = 0.5$  case, and increases for larger dipoles.

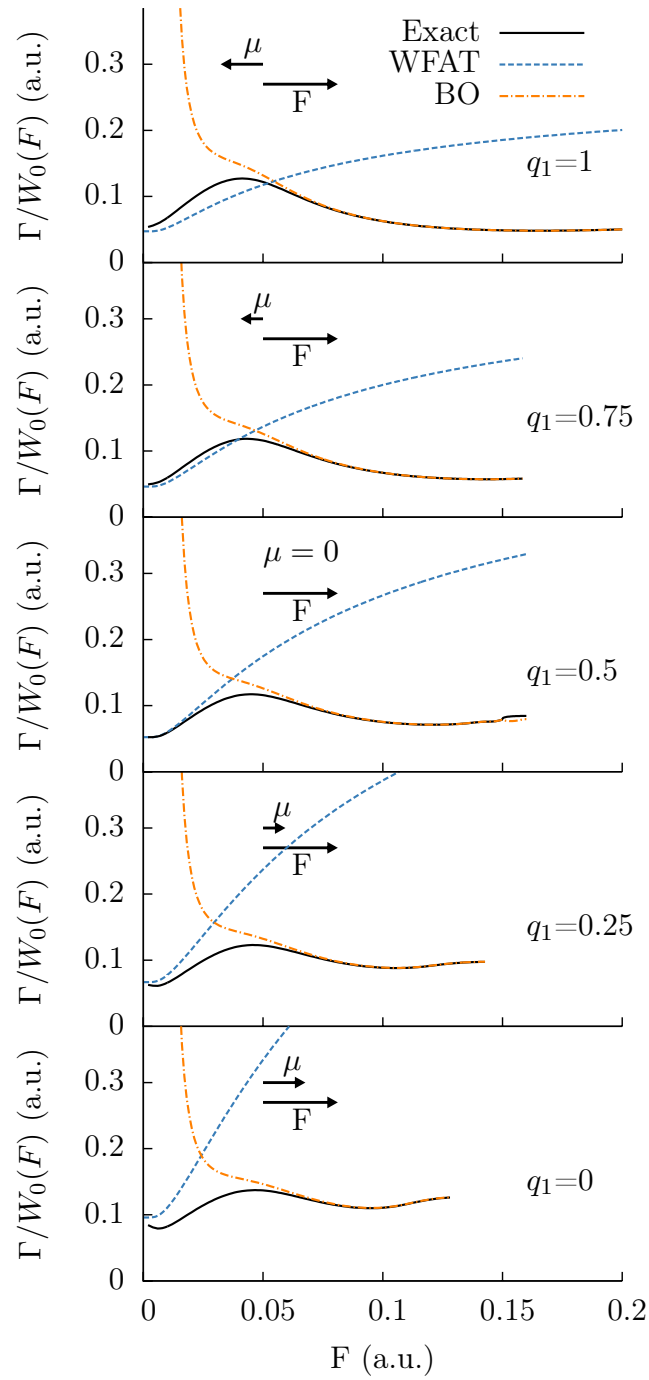


Figure 3.8: Ionization rates for different dipoles using the ctp potential. The arrows indicate the orientation of the total dipole from equation (3.33) compared to the field. Solid lines: exact rate. Dashed lines: WFAT rate. Dashed-dotted lines: BO rate.

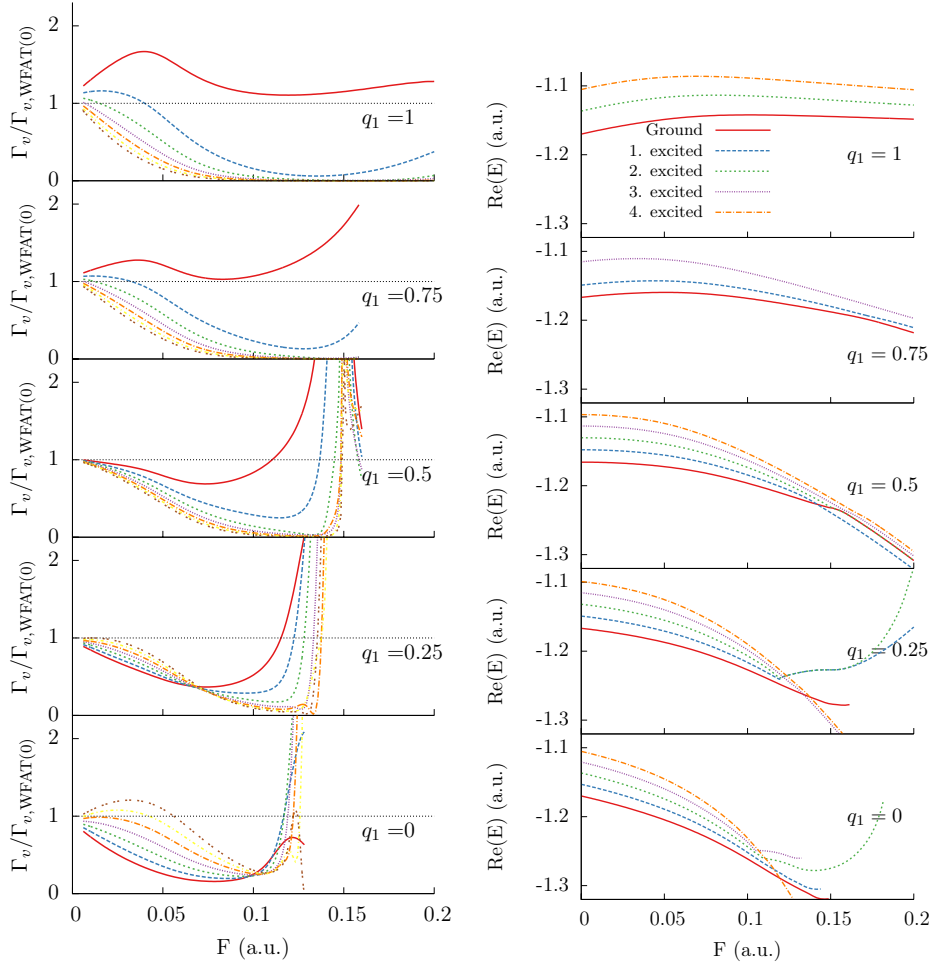


Figure 3.9: Left: Exact partial rates  $\Gamma_v = |f_v|^2$  divided by the WFAT partial rates  $\Gamma_{v,WFAT} = G_v^2 W_v(F)$ , for different dipoles using the ctp potential. The red line is the first channel, the rest follow in order. The dotted line at 1 is a guide for the eye.

Right: Real part of the energy for selected states. As  $q_1$  is decreased the energies cross at smaller values of  $F$ . The R-matrix propagation has difficulty continuing across such a crossing. Some of the states are missing from this plot because the calculation for them failed, showing the trickiness of the R-matrix propagation method.

## 4 Outlook

In the previous chapter the theory of [15] was extended to the case of non-symmetric potentials with a coulomb tail.

I am Currently working on finishing an article with content more or less corresponding to that of chapter 3. After this we plan to write a second article where the focus will be on variations of the nuclear masses. As the nuclear mass increases the BO approximation gets better, and an interval appears where WFAT and BO applies simultaneously. This might be interesting to look closer into, since the transition from a bound electron to an ionized electron in the BO picture is between different BO curves, whereas in WFAT such a transition is from a vibrational state to another vibrational state.

Which direction the project takes after this is not decided at this point. One possibility would be to include a disassociation channel. In the model potential we use now, we have a rather artificial inter-nuclear potential that goes like  $o(R^2)$  when  $R \rightarrow \infty$ . A more realistic potential would go to 0, but this has been neglected so far.

Another possibility would be to look at 3D extensions of the 1D model considered so far. Care should be taken in choosing the coordinates for this 3D model, such that the symmetries of the system can be exploited and calculation times be kept on a realistic level.

Both of these possibilities are continuations of the nuclear motion project. An entirely different possibility, unrelated to this, would be to use some of the time dependent quantum chemistry codes currently being developed in the group to look at some atomic or molecular system.

Quantum chemistry is a field concerned with describing the structure of molecules. The basic challenge in the description of molecules (and atoms) is the fact that they contain many electrons. In quantum chemistry these electrons are described using anti-symmetrized product bases of one-electron state functions, known as Slater determinants. The problem is that using a single of these Slater determinants neglects correlations of the electrons, that is, it fails to completely describe how the electrons interact with each other. One must therefore use linear combinations of

Slater determinants to describe how the electrons interact. How to choose these linear combinations is one of the main challenges in the field of quantum chemistry.

Quantum chemistry has so far mainly been concerned with finding stationary solutions of the time independent Schrödinger equation. A number of post docs in the group are working on finding ways to extend the methods of quantum chemistry to the time regime, see e.g. [6]. Using one of these codes is also a possible way to continue the project.

We have discussed the possibility of a stay abroad in the spring of 2015.

# Bibliography

- [1] B. Bransden and C. Joachain, *Physics of atoms and molecules*. Pearson Education Limited, second ed., 2003.
- [2] F. Krausz and M. Ivanov, “Attosecond physics,” *Rev. Mod. Phys.*, vol. 81, pp. 163–234, Feb 2009.
- [3] M. Feit, J. F. Jr., and A. Steiger, “Solution of the Schrödinger equation by a spectral method,” *Journal of Computational Physics*, vol. 47, no. 3, pp. 412 – 433, 1982.
- [4] M. Nest, T. Klamroth, and P. Saalfrank, “The multiconfiguration time-dependent Hartree-Fock method for quantum chemical calculations,” *The Journal of Chemical Physics*, vol. 122, no. 12, p. 124102, 2005.
- [5] W. Li and W. Xu, “Double ionization of helium studied with the multi-configuration time-dependent Hartree-Fock method,” *Molecular Physics*, vol. 111, no. 1, pp. 119–122, 2013.
- [6] H. Miyagi and L. B. Madsen, “Time-dependent restricted-active-space self-consistent-field theory for laser-driven many-electron dynamics,” *Phys. Rev. A*, vol. 87, p. 062511, Jun 2013.
- [7] J. C. Tremblay, T. Klamroth, and P. Saalfrank, “Time-dependent configuration-interaction calculations of laser-driven dynamics in presence of dissipation,” *The Journal of Chemical Physics*, vol. 129, no. 8, p. 084302, 2008.
- [8] M. Nest, F. Remacle, and R. D. Levine, “Pump and probe ultrafast electron dynamics in lih: a computational study,” *New Journal of Physics*, vol. 10, no. 2, p. 025019, 2008.
- [9] T. Nubbemeyer and U. Eichmann, “Excitation of he atoms in the strong-field tunneling regime,” *The European Physical Journal Special Topics*, vol. 222, no. 9, pp. 2267–2272, 2013.
- [10] O. I. Tolstikhin, T. Morishita, and L. B. Madsen, “Theory of tunneling ionization of molecules: Weak-field asymptotics including dipole effects,” *Phys. Rev. A*, vol. 84, p. 053423, Nov 2011.



- [11] V. H. Trinh, O. I. Tolstikhin, L. B. Madsen, and T. Morishita, “First-order correction terms in the weak-field asymptotic theory of tunneling ionization,” *Phys. Rev. A*, vol. 87, p. 043426, Apr 2013.
- [12] L. B. Madsen, O. I. Tolstikhin, and T. Morishita, “Application of the weak-field asymptotic theory to the analysis of tunneling ionization of linear molecules,” *Phys. Rev. A*, vol. 85, p. 053404, May 2012.
- [13] L. B. Madsen, F. Jensen, O. I. Tolstikhin, and T. Morishita, “Application of the weak-field asymptotic theory to tunneling ionization of H<sub>2</sub>O,” *Phys. Rev. A*, vol. 89, p. 033412, Mar 2014.
- [14] O. I. Tolstikhin, L. B. Madsen, and T. Morishita, “Weak-field asymptotic theory of tunneling ionization in many-electron atomic and molecular systems,” *Phys. Rev. A*, vol. 89, p. 013421, Jan 2014.
- [15] O. I. Tolstikhin and L. B. Madsen, “Retardation effects and the born-oppenheimer approximation: Theory of tunneling ionization of molecules revisited,” *Phys. Rev. Lett.*, vol. 111, p. 153003, Oct 2013.
- [16] J. C. Light, I. P. Hamilton, and J. V. Lill, “Generalized discrete variable approximation in quantum mechanics,” *The Journal of Chemical Physics*, vol. 82, no. 3, pp. 1400–1409, 1985.
- [17] K. Baluja, P. Burke, and L. Morgan, “R-matrix propagation program for solving coupled second-order differential equations,” *Computer Physics Communications*, vol. 27, no. 3, pp. 299 – 307, 1982.
- [18] O. I. Tolstikhin and C. Namba, *CTBC: A Program to Solve the Colinear Three-body Coulomb Problem; Bound States and Scattering Below the Three-body Disintegration Threshold*. National Institute for Fusion Science, 2003.
- [19] O. I. Tolstikhin, S. Watanabe, and M. Matsuzawa, “‘slow’ variable discretization: a novel approach for hamiltonians allowing adiabatic separation of variables,” *Journal of Physics B: Atomic, Molecular and Optical Physics*, vol. 29, no. 11, p. L389, 1996.
- [20] P. A. Batishchev, O. I. Tolstikhin, and T. Morishita, “Atomic siegert states in an electric field: Transverse momentum distribution of the ionized electrons,” *Phys. Rev. A*, vol. 82, p. 023416, Aug 2010.
- [21] H. Wind, “Electron energy for H<sub>2</sub><sup>+</sup> in the ground state,” *The Journal of Chemical Physics*, vol. 42, no. 7, pp. 2371–2373, 1965.
- [22] W. Kołos and L. Wolniewicz, “Accurate adiabatic treatment of the ground state of the hydrogen molecule,” *The Journal of Chemical Physics*, vol. 41, no. 12, pp. 3663–3673, 1964.